BIOCHEMISTRY
including biophysical chemistry & molecular biology

Article

pubs.acs.org/biochemistry

Retinal Ligand Mobility Explains Internal Hydration and Reconciles Active Rhodopsin Structures

Nicholas Leioatts,[†] Blake Mertz,[‡,@] Karina Martínez-Mayorga,[‡,#] Tod D. Romo,[†] Michael C. Pitman,[§,▽] Scott E. Feller,[∥] Alan Grossfield,*[,†] and Michael F. Brown*[,‡,⊥]

[†]Department of Biochemistry and Biophysics, University of Rochester Medical Center, Rochester, New York 14642, United States
[‡]Department of Chemistry and Biochemistry, University of Arizona, Tucson, Arizona 85721, United States
[§]IBM T. J. Watson Research Center, Yorktown Heights, New York 10598, United States
[∥]Department of Chemistry, Wabash College, Crawfordsville, Indiana 47933, United States
[⊥]Department of Physics, University of Arizona, Tucson, Arizona 85721, United States

W *Web-Enhanced Feature* *S* *Supporting Information*

ABSTRACT: Rhodopsin, the mammalian dim-light receptor, is one of the best-characterized G-protein-coupled receptors, a pharmaceutically important class of membrane proteins that has garnered a great deal of attention because of the recent availability of structural information. Yet the mechanism of rhodopsin activation is not fully understood. Here, we use microsecond-scale all-atom molecular dynamics simulations, validated by solid-state ^{2}H nuclear magnetic resonance spectroscopy, to understand the transition between the dark and metarhodopsin I (Meta I) states. Our analysis of these simulations reveals striking differences in ligand flexibility between the two states. Retinal is much more dynamic in Meta I, adopting an elongated conformation similar to that seen in the recent activelike crystal structures. Surprisingly, this elongation corresponds to both a dramatic influx of bulk water into the hydrophobic core of the protein and a concerted transition in the highly conserved Trp265$^{6.48}$ residue. In addition, enhanced ligand flexibility upon light activation provides an explanation for the different retinal orientations observed in X-ray crystal structures of active rhodopsin.

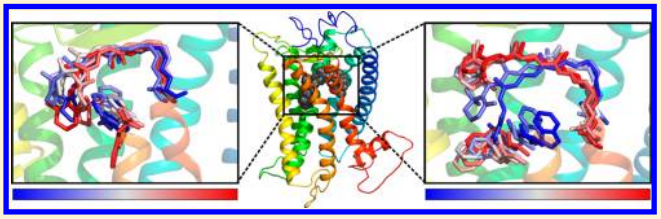

With an estimated 800 members, the family of G-protein-coupled receptors (GPCRs) constitutes the largest class of proteins in humans.[1] They are involved in a wide range of cell processes,[2−4] including visual[5] and olfactory[6,7] reception and neurotransmission.[7−9] As the most widespread targets of small-molecule drugs,[9,10] GPCRs are of vital biomedical importance. Understanding their mechanism of activation at an atomic level is a primary goal of both pharmaceutical and academic researchers.[2−4,8−11] They act as molecular transducers, passing signals across the cell membrane through an allosteric activation process. Signaling is modulated by extracellular ligands, while G-protein activation occurs inside the cell by coupling to the cytoplasmic face of the GPCR within the lipid bilayer.

Rhodopsin, a class A GPCR, is one of the best biophysically characterized proteins in this family.[2,12] As a result, it is often used as a model system, although it is somewhat atypical. In contrast to most GPCRs, which are activated by diffusible agonists, rhodopsin's ligand, retinal, is covalently bound to the protein by a Schiff base linkage to Lys296$^{7.43}$ (superscripts denote Ballesteros and Weinstein's conservation-based residue numbering[13]). Retinal acts as both an inverse agonist and a full agonist.[14] These two functions are achieved through the ligand's ability to take on alternate stable conformations when bound to the receptor. In the dark state of rhodopsin, 11-*cis*-retinal is bound to the inactive protein. Upon absorption of a photon, the C11═C12 torsion is isomerized, yielding the all-*trans* retinylidene ligand, which is a powerful agonist.[15] This motion facilitates activation through a series of spectroscopically distinct intermediates.[16] The first four metastable states along the nonequilibrium path, namely, bathorhodopsin, the blue-shifted intermediate, lumirhodopsin, and metarhodopsin I (Meta I), are unable to activate G-proteins, but Meta I exists in equilibrium with the active state, metarhodopsin II (Meta II). Understanding the dynamics of the Meta I to Meta II transition at the atomic level has garnered much attention because this equilibrium relates to GPCR activation in general.[3,4]

In 2000, the first crystal structure of dark-state rhodopsin was published, making high-resolution experimental coordinates of a GPCR available for the first time.[17] Since then, X-ray crystal structures have been reported for most photoproduct intermediates. These include the intermediates that are structurally and functionally inactive: the dark,[17,18] bathorhodopsin,[19] and lumirhodopsin[20] states. Proposed structures of Meta II and constitutively active states,[21−23] and the structurally similar apoprotein, opsin,[24,25] have also been

Received: October 11, 2013
Revised: December 6, 2013
Published: December 12, 2013

published. The overall protein conformations in these structures are quite similar and show the expected[26] conformational transitions, including elongation of transmembrane helix 5 (H5) and an outward tilt of helix 6 (H6) (Figure 1a).

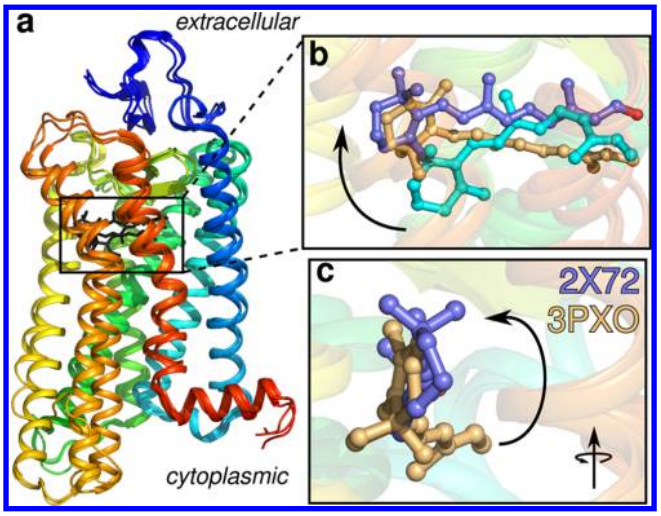

Figure 1. Comparison of X-ray crystal structures of rhodopsin in the inactive and active states. Coordinates were obtained from the Protein Data Bank (entries 1U19,[18] 2X72,[21] and 3PXO[22]). (a) Overall structure of rhodopsin (rainbow cartoon representation) with retinal in the binding pocket (black sticks). The figure is oriented with the extracellular side (intradiscal) at the top. The protein conformation is similar in both active structures. (b) Close-up of the binding pocket that reveals a ligand more elongated in the active structures (purple and tan) than in the inactive dark structure (cyan). (c) View after a 90° rotation in the plane of the membrane that shows the two retinal orientations in the active structures. Note that retinal differs by a long-axis flip of 180° between these two structures.

However, retinal appears in two distinct conformations in the published crystal structures of active opsin.[21,22] Both research groups report an elongated ligand (Figure 1b), but surprisingly, one structure[22] contained a long-axis flip, with retinal rotated by nearly 180° (Figure 1c). One possible explanation for this discrepancy, a Glu113Gln$^{3.28}$ mutation, has been addressed.[23] Here, we propose that the ligand becomes more flexible after isomerization, which may also reconcile the inconsistency between the two previously published structures.[21,22] Understanding the dynamics of the Meta I intermediate is crucial not only for understanding rhodopsin activation, but also for applying rhodopsin-based models to other GPCRs.[27−35] Because Meta I is in equilibrium with the active Meta II state, it is likely the intermediate most representative of the inactive state in other GPCRs. In this view, dark-state rhodopsin is more comparable to a canonical GPCR bound to a strong inverse agonist.[14]

We have employed atomistic molecular dynamics (MD) simulations that were validated by ^{2}H solid-state NMR[36] (ssNMR) spectroscopy to understand the transition from dark-state rhodopsin to Meta I. As in our preliminary work,[36] we calculated the ^{2}H NMR spectra of the three methyl groups of the retinylidene ligand[37] and compared the spectra to experimental data. Previously, we found that our data corroborated a proposed complex-counterion mechanism for rhodopsin activation.[38,39] This mechanism asserts that both Glu113$^{3.28}$ and Glu181^{EL2} are deprotonated throughout the activation process, giving the binding pocket a net negative charge.[38,39] In the work presented here, we expand this data set to include a comparison between dark-state experimental and simulation data. We show how simulations of the dark state and complex-counterion mechanism reveal the dynamics involved in the early stages of rhodopsin activation. Most strikingly, our analysis shows key differences in the structure and dynamics of retinal. During activation, the ligand undergoes a concerted transition and elongation similar to that seen experimentally.[21,22,27,40] This transition also includes conformational changes involving a highly conserved tryptophan (Trp265$^{6.48}$) and is followed by a surprisingly dramatic increase in the level of internal hydration of the protein.[41] Moreover, the Schiff base-linked lysine (Lys296$^{7.43}$) is more dynamic after retinal isomerization, with several torsions adopting new conformations. We show that cooperative motion of retinal together with these two residues accounts for almost one-third of the dominant motion of the binding pocket in the complex-counterion simulation. Notably, this elongation and increased flexibility help reconcile the distinct conformations of retinal in the binding pocket published recently[21−23] (Figure 1b,c), as well as the multiple occupancies noted in one of the structures.[21] Our analysis shows that dynamics, in addition to structure, are important for understanding how light-induced isomerization of a bound ligand yields activation of this prototypical GPCR.

METHODS

Molecular Dynamics Simulations. The methodological details of these simulations have been reported elsewhere,[36,42] and here we describe the construction and composition of the system only briefly. The specific setup for simulating the complex-counterion and counterion-switch mechanisms is discussed in the Supporting Information. The starting coordinates for all three simulations were obtained from previously published data.[43] The protein was embedded in a bilayer containing 50 molecules of 1-stearoyl-2-docosahexaenoyl-*sn*-glycero-3-phosphoethanolamine (SDPE), 49 molecules of 1-stearoyl-2-docosahexaenoyl-*sn*-glycero-3-phosphocholine (SDPC), and 24 molecules of cholesterol. The system was hydrated with 7400 TIP3P water molecules. We added 14 Na^+ and 16 Cl^- atoms to neutralize the system and obtain a salt concentration of approximately 100 mM. The resulting systems were then simulated on IBM Watson's BlueGene/L computer using Blue Matter[44] in the *NVE* ensemble with an average temperature of 311 K. The CHARMM27 force field[45] was used for the protein with updated lipid/cholesterol parameters.[46] Retinal parameters were obtained from Nina et al.[47] A time step of 2 fs was used with the RATTLE algorithm[48] applied to constrain hydrogen bonds. Electrostatic interactions were computed using the particle−particle particle−mesh Ewald method[49] with a 128 × 128 × 128 grid. Van der Waals interactions were smoothly truncated by force switching from 9 to 10 Å.

Simulation Analysis. Analysis of the MD simulations was performed in LOOS[50] (version 2.0, loos.sourceforge.net). LOOS is a lightweight, object-oriented MD simulation analysis package. It facilitates user-developed tools by handling much of the syntactical overhead and interfaces with all major MD packages. As in previous work, simulations were compared to experiment by computing the theoretical ^{2}H ssNMR spectra from molecular dynamics trajectories.[36] The method for fitting the experimental mosaic spread was reimplemented within the LOOS framework. A detailed description of the analysis

dx.doi.org/10.1021/bi4013947 | *Biochemistry* 2014, 53, 376−385

together with the ssNMR details can be found in the Supporting Information. We emphasize that whenever possible, it is preferable to compute an experimental observable from the simulation, in this case the NMR spectrum, instead of comparing the simulation to the interpretation of experimental data, because such an interpretation often requires limiting assumptions (e.g., the existence of a single dominant conformation).[42]

Principal component analysis was performed by first calculating the average structure using an iterative alignment procedure.[51,52] Specifically, matrix diagonalization was performed using singular-value decomposition. This approach makes it trivial to calculate the time series of displacements along the modes, called the right singular vectors. Water density calculations were also performed with tools implemented in LOOS. After the protein had been aligned, waters were histogrammed over the trajectory into discrete bins and normalized to bulk density (calculated from a region of the system with no protein or lipids). This three-dimensional grid was then convolved with a Gaussian kernel and written as an electron density map. Images and movies were made with LOOS and rendered in PyMOL (version 1.4.1, http://www.pymol.org). All data were plotted with gnuplot (version 4.4, http://www.gnuplot.info).

RESULTS

A combination of three independent all-atom simulations of rhodopsin totaling 5 μs were used to describe the dynamics of retinal during the early stages of protein activation. The simulations included a 1.6 μs trajectory of dark-state rhodopsin (containing 11-*cis*-retinal) and two rhodopsin trajectories conducted using an isomerized all-*trans*-retinal, each in an explicit bilayer.[38,41] The details of the 11-*cis*- to all-*trans*-retinal isomerization can be found in the Supporting Information and constitute an interesting area of ongoing computational research.[53−55] Specifically, we compared experimental ^{2}H ssNMR spectra of Meta I rhodopsin to simulations of the counterion-switch and complex-counterion mechanism in earlier work.[36] The study presented here extends our previous analysis to include a comparison of dark-state experimental and simulation spectra (Figure 2 and Figures S1−S7 of the Supporting Information). Analyzing the dark state of the receptor provides a vital control, something not often seen in computational work. Moreover, we expand on previous work, analyzing the functional motions within the binding pocket and demonstrating how these motions can reconcile the alternative configurations of retinal seen in recent crystal structures of the active Meta II state.

Simulation and NMR Data Corroborate the Complex-Counterion Hypothesis. We focused our study on the large-scale reorientations of the ligand in the binding pocket over microsecond time scales, as they pertain to the formation of the Meta I intermediate. As in our earlier work, we validated the simulations by comparing them to experimental ^{2}H ssNMR data. The orientations of the C5-, C9-, and C13-methyl groups were measured using oriented samples of rhodopsin in both the dark state and Meta I (Figure 2). The positions of the three methyl groups are illustrated for reference in Figure 2a. Despite the similarity between experimental data sets, we were able to interpret the small differences in the theoretical spectra computed from the dark-state and Meta I simulations. Spectra calculated from the three simulations were compared for two different ssNMR experimental data sets (Figure 2b−g): dark-state rhodopsin in the left column and Meta I in the right column. For the sake of additional clarity, the data shown in these panels are all reproduced in Figures S1−S7 of the Supporting Information. Spectra are shown for all seven sample tilt angles obtained experimentally and computationally.[40] Data from the dark-state simulation were compared to both experimental conditions: retinal in the dark state (Figure 2b) or Meta I (Figure 2c). Theoretical spectra from the dark-state simulation match the experiment well (Figure 2b) but are also quite similar to retinal's conformation in Meta I rhodopsin (Figure 2c). This result was anticipated because the experimental spectra were very similar (Figure S1 of the Supporting Information). However, the C9-methyl spectra calculated from the dark-state simulation reproduce the dark-

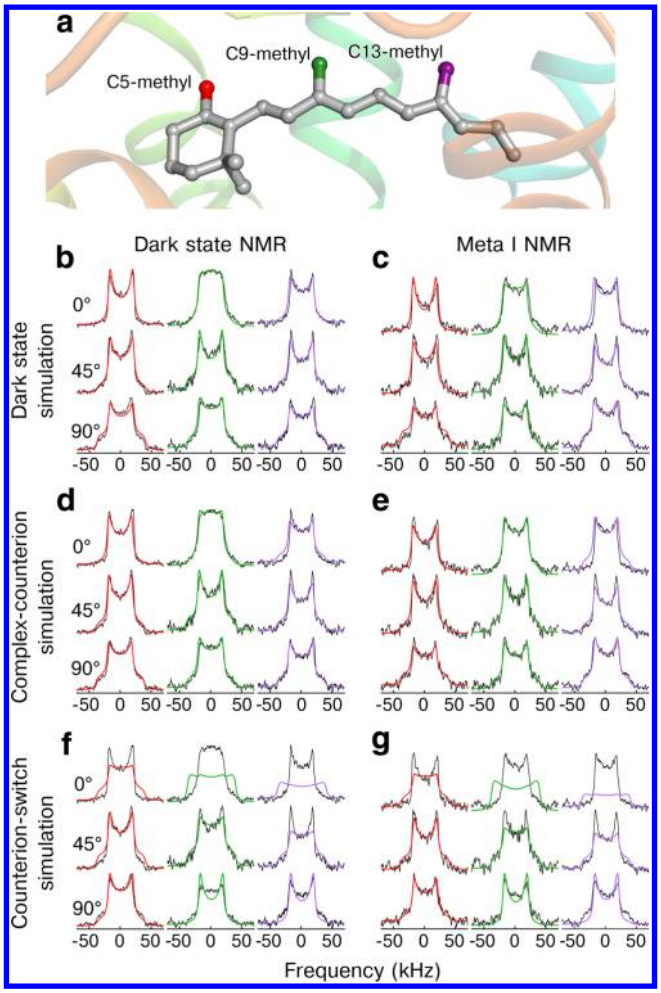

Figure 2. Solid-state ^{2}H NMR spectra calculated from molecular dynamics (MD) simulations corroborate complex-counterion mechanism of rhodopsin activation. (a) Schematic of retinal (gray) in its binding pocket. Carbon atoms of retinal are colored as follows: (red) C5-methyl, (green) C9-methyl, and (purple) C13-methyl. This coloring is used in panels b−g for the simulation-based line shape calculations. (b−g) Solid-state ^{2}H NMR spectra computed from MD simulations (color) plotted with experimental data (black). Each row of data in a panel indicates a different orientation of the bilayer to the magnetic field: 0° (first row), 45° (second row), and 90° (third row). The full series of tilt angles can be seen in Figures S2−S7 of the Supporting Information. Spectra were calculated from the dark-state (b and c), complex-counterion (d and e), and counterion-switch (f and g) simulations. These were compared to the dark-state (b, d, and f) and Meta I (c, e, and g) experimental ^{2}H ssNMR spectra.

dx.doi.org/10.1021/bi4013947 | *Biochemistry* 2014, 53, 376−385

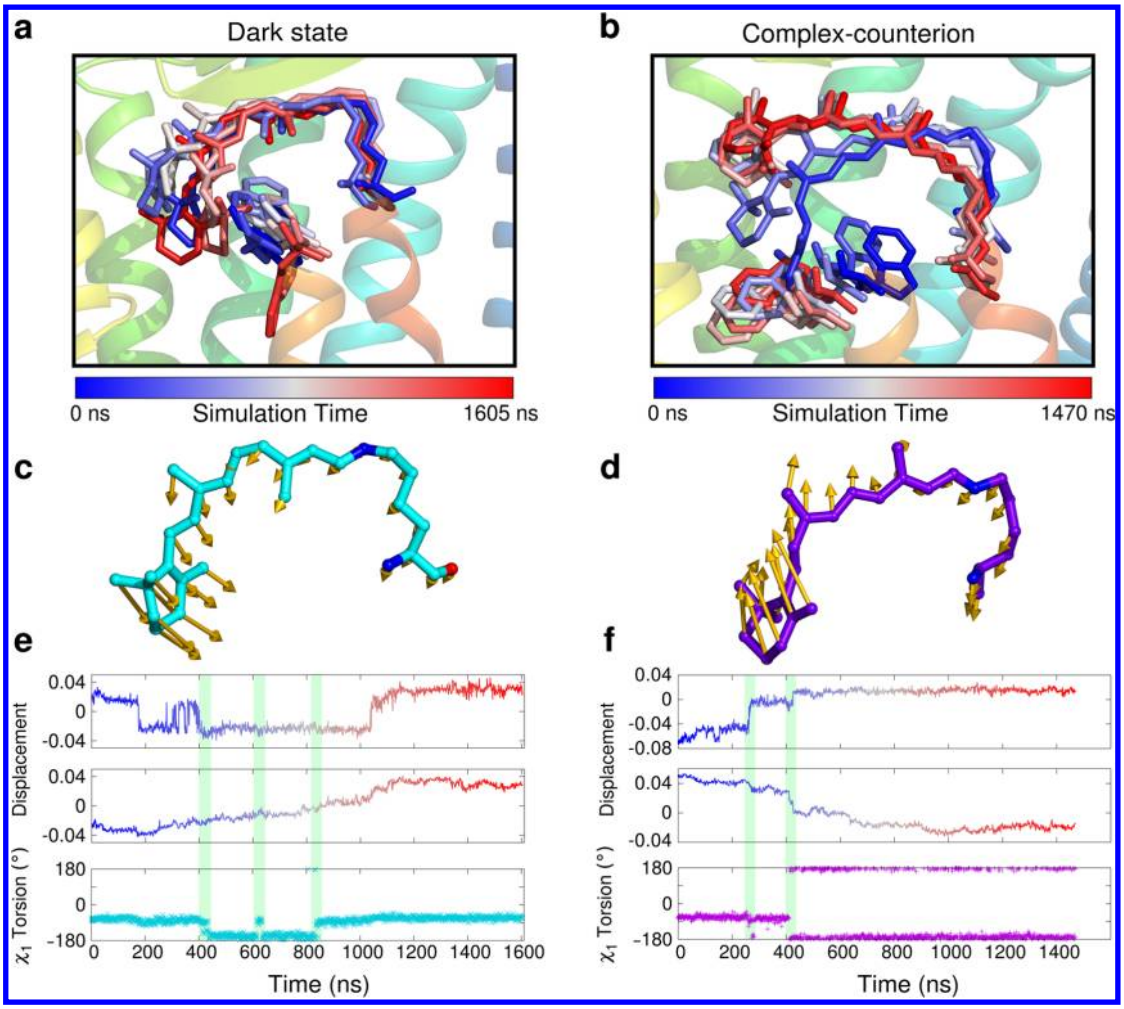

Figure 3. Retinal makes a concerted transition and is elongated early in rhodopsin's activation. Results are shown from (left) the dark-state and (right) complex-counterion simulations. (a) Close-up of the ligand binding pocket that shows retinal, Lys296$^{7.43}$, and Trp265$^{6.48}$ motion in the dark-state simulation. Atomic coordinates were taken over the course of the trajectory at equal time intervals progressing from blue to white to red (time bar shown below). The position of the ligand can be seen with respect to rhodopsin transmembrane helices (the extracellular portions of H6 and H7 have been removed for the sake of clarity). Rhodopsin is colored as in Figure 1. (b) Expanded view of the retinal binding pocket for the complex-counterion trajectory. As in panel a, retinal, Lys296$^{7.43}$, and Trp265$^{6.48}$ are plotted as the simulation progressed. (c) 11-*cis*-retinal's (cyan) most concerted motion is shown for the dark-state simulation. The principal component of motion is shown as yellow sticks superimposed on the average structure of retinal. (d) All-*trans*-retinal's (purple) principal component of motion (yellow sticks) is shown for the complex-counterion simulation. (e) Displacement of 11-*cis*-retinal and Lys296$^{7.43}$ along the first principal component for the dark-state simulation. This displacement is calculated using the average structure. In the top panel, the displacement along the principal component of motion in panel c is illustrated as a function of simulation time. The coloring matches the progression of time shown in panel a. The middle panel shows the time course of displacement where the principal component analysis has been expanded to include the entire binding pocket (see Results). The bottom panel shows the time series of the χ_1 torsion of Trp265$^{6.48}$. (f) Displacement of all-*trans*-retinal and Lys296$^{7.43}$ along the first principal component of motion during the complex-counterion simulation. The top panel shows the displacement along the principal component (as shown in panel d). The middle panel shows the displacement along the principal component where the PCA is expanded to include the entire binding pocket (see Results). The bottom panel shows the time series of the χ_1 torsion of Trp265$^{6.48}$.

state experimental spectra better than those calculated from Meta I experiments.

The complex-counterion simulation was also compared to both experiments (Figure 2d,e). Here, retinal also produced spectra that are similar to both experimental data sets, but there are notable differences. The C9-methyl spectrum calculated from simulation data shows some splitting of the doublet at a 0° sample tilt (Figure 2d, top middle spectrum), while the peaks were merged in the experimental spectrum. By contrast, the dark-state simulation spectrum produced a broad peak (Figure 2b, top middle). Because the experimental spectra are very similar in the dark state and Meta I, it is not surprising that the simulated spectra cannot distinguish between them. Importantly, the spectra calculated from the counterion-switch simulation (Figure 2f,g) do not reproduce either experimental result. On the basis of this finding, we focus our comparisons on the dark-state and complex-counterion simulations, but not the counterion-switch simulation.

Rhodopsin Activation Involves Collective Motion of the Ligand Binding Pocket. The transition from the dark state to Meta I does not involve large-scale rearrangement of the protein,[28] in contrast to Meta II (see Figure 1a). Rather, it appears that the conformational changes are localized to the binding pocket, and serve to prime the protein for the transition to the active Meta II structure. Accordingly, we analyzed the concerted dynamics of retinal within the binding

dx.doi.org/10.1021/bi4013947 | *Biochemistry* 2014, 53, 376−385

pocket (Figure 3). Interestingly, retinal is shown in very different conformations in the recent Meta II crystal structures.[21−23] Both laboratories report a ligand elongation of >4 Å; however, Choe et al.[22] show retinal flipped by 180° about its polyene tail (Figure 1c). This result will be further addressed below.

Notably, inspection of the dark-state simulation shows comparatively little retinal motion (Figure 3a). Trp265$^{6.48}$ is also relatively rigid until it undergoes a χ_2 torsion flip in the last 500 ns (Figure S8 of the Supporting Information). The behavior is quite different in the complex-counterion simulation; retinal translates "upward" toward the extracellular (intradiscal) face of the protein (Figure 3b), similar to what appears in the active crystal structures (represented here in Figure 1b). During this transition, Trp265$^{6.48}$ rotates about its χ_1 torsion to occupy the space vacated by retinal's β-ionone ring, as previously hypothesized[56,57] and seen in the cyro-electron microscopy structure.[28]

Somewhat surprisingly, retinal's overall flexibility is comparable in the two simulations (the maximal self-root-mean-square deviation was 1.48 Å in the dark-state simulation and 1.51 Å in the complex-counterion simulation, based on an iterative alignment of the transmembrane α-carbons), but the dynamics are quite different. This may be because the isomerized retinal was in a more unfavorable orientation. To quantify these differences in dynamics, we applied more sophisticated analysis methods. We used principal component analysis (PCA) to derive a reduced set of functionally important motions. The largest collective motions in retinal and its Schiff base-linked lysine are shown for the dark-state and complex-counterion simulations in panels c and d of Figure 3. In the dark-state simulation (Figure 3c), the motion is dominated by a fluctuation of the β-ionone ring toward transmembrane helix H6 and in particular Trp265$^{6.48}$, which is located closer to the cytoplasmic face than retinal. This is in stark contrast to the upward transition that dominates retinal motion in the complex-counterion simulation (Figure 3d). In addition, retinal is elongated in the complex-counterion simulation, moving the β-ionone ring away from Trp265$^{6.48}$ as compared to the dark-state simulation.

Dynamics of Retinal and Tryptophan-265 Are Correlated. Next, we used these principal components of motion to further investigate the correlation between the rotameric orientation of Trp265$^{6.48}$ and retinal dynamics. We plotted the projection of each MD trajectory on its first principal component to improve our understanding of the transitions made in the two simulations, and to assess the possibility of their correlation with Trp265$^{6.48}$ dynamics. First, we did this just for retinal and its attached lysine (Figure 3e, top panel). Including Lys296$^{7.43}$ is important as this side chain is very flexible, and its motions directly impact retinal's orientation. Additionally, the side chain adopted very different structures between the two simulations. A number of transitions occurred in the first half of the simulation, indicating structural reorganization along this mode of motion (Figure 3e, top panel). This analysis was then extended to the entire binding pocket, defined as residues within 7 Å of retinal in the starting structure (Figure 3e, middle panel). Viewed this way, the data show no single transition event, but rather a smooth displacement along the principal axis, lasting from 200 to 1200 ns. We also monitored the χ_1 torsion orientation of Trp265$^{6.48}$ throughout the dark-state simulation, where four rotameric flips occur (Figure 3e, bottom panel). However, none of these torsions appreciably displaced the tryptophan side chain (Figure 3a), nor were their transitions concurrent with those of either PCA result (Figure 3e, top and middle). This is illustrated by the green bars (Figure 3e), which are placed over the χ_1 torsion changes in Trp265$^{6.48}$.

To further quantify the binding pocket dynamics from the complex-counterion simulation, we projected the trajectory onto the principal axis of motion (Figure 3f, top and middle). This analysis revealed two rapid transitions by retinal and lysine (Figure 3f, top), the second of which is also prevalent in the PCA of the entire binding pocket (Figure 3f, middle). Physically, these motions are related to the upward transition of retinal toward EL2, and the side chain reorientation of Trp265$^{6.48}$. Together, retinal and Trp265$^{6.48}$ contribute 28% of the most concerted motion in the binding pocket (that is, they make up 28% of principal component 1). This result is striking, as they represent only 30 of the 650 heavy atoms (or 5%) used in the PCA calculation. In addition, the χ_1 torsional orientation of Trp265$^{6.48}$ was tracked for this trajectory (Figure 3f, bottom). Again, the complex-counterion simulation is notably different from the dark state. Here, tryptophan undergoes three χ_1 transitions, which leaves it in the *trans* conformation. These rotameric reorientations coincide with the dominant transitions revealed from both PCA calculations (Figure 3f, green bars). Notably, the χ_1 torsion of Trp265$^{6.48}$ occupies a predominantly *trans* conformation in the complex-counterion simulation. The PCA of retinal and lysine alone reveals two transitions (Figure 3f and Video S1). The first occurs at ∼300 ns and coincides with the elongation and much of the upward translation of the ligand. The second, which happens ∼125 ns later, is a smaller translation that brings the β-ionone ring closer to the cap formed by EL2, where it stays for the remainder of the simulation. This movement is accompanied by the long-lived torsional flip in Trp265$^{6.48}$. The PCA of the binding pocket showed similar results, but here the magnitude of the two transitions was reversed. The first transition at ∼300 ns was relatively small. The second transition (at ∼425 ns) occurred as the β-ionone ring continued upward and the tryptophan's side chain was reoriented.

Water Influx Accompanies the Concerted Motion of Retinal in the Binding Pocket. Structural water in the hydrophobic core of GPCRs was seen in the earliest crystal structure,[17] leading to predictions that they connect the motions of distant parts of the protein and facilitate activation, acting as hydrogen bonding partners.[58−61] Interestingly, bulk internal water may also play a role in the later stages of activation.[62] As described previously, there was an influx of water into the core of rhodopsin after retinal isomerization, a result also supported by ssNMR data.[41] This increase in the level of hydration can be seen in the complex-counterion simulation but not the dark-state simulation (Figure 4a). The level of internal hydration is comparable at the beginning of the simulations but begins to increase 425 ns into the complex-counterion trajectory, after the ligand undergoes its largest concerted motion. The water density from this simulation is visualized before 250 ns (Figure 4b) and after 450 ns (Figure 4c), when the major transition occurred. The increase in the level of internal hydration can also be seen in the time evolution of the complex-counterion simulation (Video S2). Relatively little water starts in the hydrophobic core of the protein, but as the simulation progresses, the level of hydration increases, nearly forming a channel through the protein.

dx.doi.org/10.1021/bi4013947 | *Biochemistry* 2014, 53, 376−385

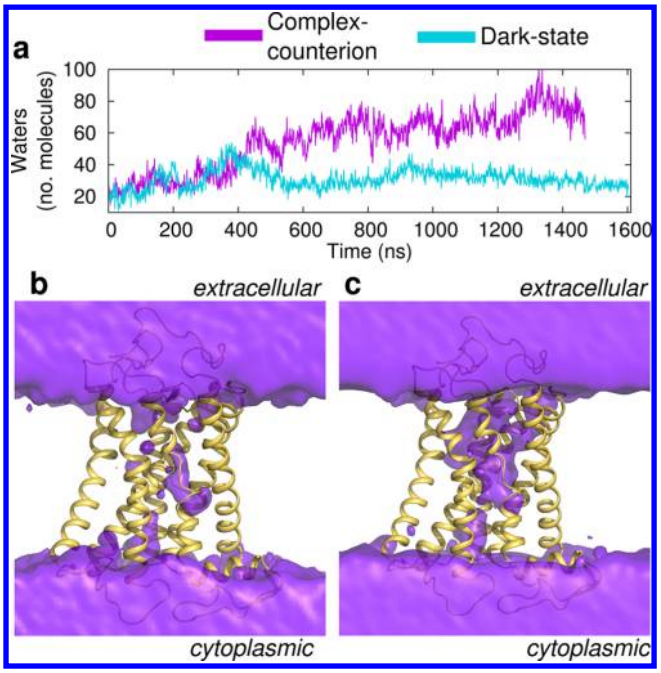

Figure 4. Complex-counterion simulation that shows the influx of bulk water into the hydrophobic core of the protein upon activation. (a) The number of water molecules within 7 Å of transmembrane residues was plotted for both the dark-state (cyan) and complex-counterion (purple) simulations. (b and c) Water density in the complex-counterion simulation averaged (b) from 100 to 250 ns and (c) from 450 to 1470 ns.

Retinal Adopts an Elongated Conformation during Activation. Notably, retinal's principal component of motion was distinct in the two trajectories, but the ligand was hardly static in the dark-state trajectory. To improve our understanding of the differences after isomerization, we next turn to the ligand's internal dynamics. In the complex-counterion simulation, retinal and Lys296$^{7.43}$ were more flexible than in the dark state, making many torsional transitions (Figure 5). A schematic depiction of the heavy atoms in retinal and lysine (Figure 5a) shows the torsion angles as the dark-state (cyan) and complex-counterion (purple) simulations progressed. The largest changes in dynamics are seen in lysine torsions. These bonds, which directly impact the orientation of retinal, are more dynamic in the complex-counterion simulation, often adopting conformations that are not seen in the dark-state trajectory. Specifically, the χ_1, Cδ−Cε, and Cε−Nζ torsions adopt different preferred orientations, which allows retinal to assume distinct conformations in the two simulations. The differences also go beyond a simple conformational preference; all lysine torsions show many more transitions in the complex-counterion simulation.

Other noteworthy changes include the C11═C12 torsion, which has been isomerized from *cis* (0°) in the dark-state simulation to *trans* (180°) in the complex-counterion simulation. This torsional reorientation changes retinal from an inverse agonist to a full agonist.[15,27] In addition, the C6−C7 torsion, where the β-ionone ring joins the retinal chain, is quite dynamic in both simulations but adopts distinct preferred conformations. Retinal elongation, which has previously been noted experimentally,[21,22,27,40] can be clearly seen in plots of the distance between the Lys296$^{7.43}$ α-carbon and the C3 atom in retinal's β-ionone ring (Figure 5b). The dark-state simulation (cyan) shows a slight elongation from 12 to 14 Å for the first 1000 ns but returns to its original value for the last 600 ns. By contrast, the complex-counterion simulation exhibits a 6 Å stretch from 12 to 18 Å. This elongation is complete within the first 450 ns, where the concerted transitions occur (Figure 3f), and is retained thereafter.

DISCUSSION

By combining computational and experimental techniques, we were able to describe the dynamics of retinal in the early stages of rhodopsin activation. One of our most significant findings was the flexibility and concerted motions made by retinal in the binding pocket. Simulations of the dark state and complex-counterion mechanism uncovered remarkable differences. Enhanced flexibility in the complex-counterion simulation, particularly in the Lys296$^{7.43}$ torsions, also provides an explanation for the surprising disparity in retinal orientation seen in the two recently published crystal structures,[21,22] as illustrated in Figure 1b,c. Using the complex-counterion simulation, we explored how the ligand dynamics change between the dark and light-activated states. After isomerization, retinal engaged in large-scale concerted movements that involved the reorientation of functionally critical residues in the binding pocket. Our results highlight these differences by comparing the complex-counterion simulation to the dark-state simulation (Figure 3). The combination of computational and experimental dark-state data provided a crucial control by describing the conformational ensemble before retinal isomerization. Ligand motion in the dark state was very subtle, which was in stark contrast to the large translation seen in the complex-counterion simulation.

Retinal Elongation Is Concerted with Binding Pocket Dynamics. In the complex-counterion simulation, retinal's β-ionone ring moved toward the extracellular (intradiscal) side of the protein, allowing Trp265$^{6.48}$ to undergo a χ_1 torsional flip (Figure 3b,f and Video S1). This highly conserved residue exhibited a similar orientation in a cryo-electron microscopy structure[28] and recent NMR data.[35] Notably, Trp265$^{6.48}$ may be functionally important; it has been implicated in the rotamer toggle switch mechanism of GPCR activation.[4,56,57] The torsional transition of this tryptophan in the complex-counterion simulation occurred with the retinal elongation, and both movements contributed remarkably to the most concerted motion seen in the simulation (Figure 3d,f). In fact, the tryptophan side chain moves into the region vacated by retinal's β-ionone ring. After the transition, this orientation was then stable for the remainder of the trajectory (~1 μs). Although Trp265$^{6.48}$ also underwent χ_1 torsion flips in the dark-state simulation, the side chain was not appreciably displaced (Figure 3a) because of compensating rotations around the χ_2 torsion (Figure S8 of the Supporting Information). These transitions were also comparably short-lived (~200 ns). Finally, 800 ns into the dark-state trajectory, Trp265$^{6.48}$ adopted its original χ_1/χ_2 torsional orientation, but the side chain was later displaced by rotation about the χ_2 torsion approximately 300 ns later (Figure 3a and Figure S8 of the Supporting Information). None of the Trp265$^{6.48}$ torsional reorientations in the dark-state simulation aligned with the ligand transitions revealed by PCA (Figure 3e and Figure S8 of the Supporting Information).

Another surprising characteristic of the complex-counterion simulation was a dramatic increase in the level of internal hydration. In our trajectories, no increase is seen in the dark-state simulation (Figure 4a). Significantly, the increase seen in

dx.doi.org/10.1021/bi4013947 | *Biochemistry* 2014, 53, 376−385

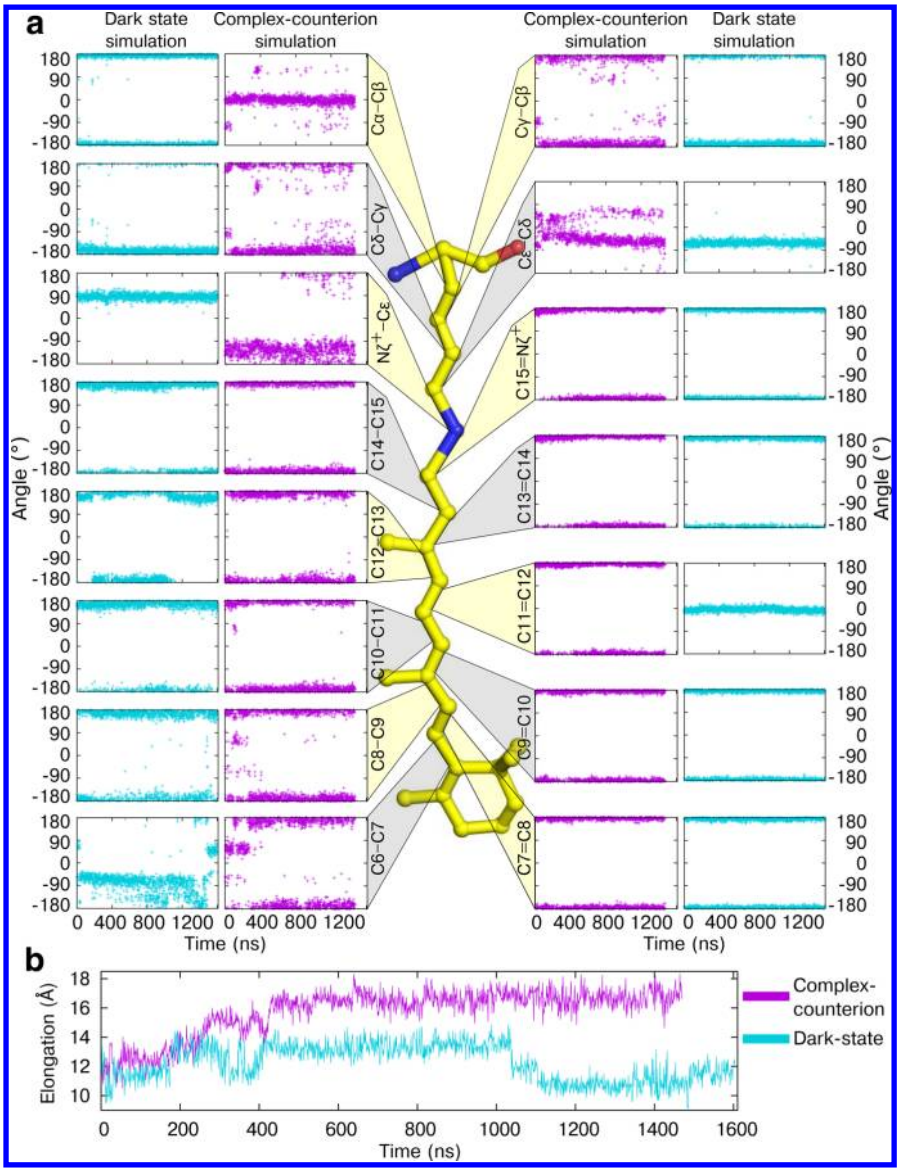

Figure 5. Retinal mobility is increased in the complex-counterion simulation. (a) Illustration of retinal and its Schiff base-linked lysine (Lys296$^{7.43}$) (carbons colored yellow and nitrogens blue). The β-ionone ring is located at the bottom of the image. The breakouts show each torsion angle plotted as a function of trajectory time for both the dark-state (cyan) and complex-counterion (purple) simulations. Each torsion is labeled by the two atoms involved, with a single dash (—) representing a single bond and a double dash (═) representing a double bond. (b) Retinal elongation is shown for both the dark-state and complex-counterion simulations. The distance between the Lys296$^{7.43}$ α-carbon and C3 in retinal's β-ionone ring is plotted for both simulations.

the complex-counterion simulation happened mostly after retinal had been elongated (Figure 4b,c). Water appeared to enter the protein from both the extracellular and cytoplasmic sides, creating a nearly continuous surface through the protein (Video S2). The level of water density is quite stable, especially for those molecules penetrating the cytoplasmic side of the protein. This is interesting, as it is well-known that bulk internal water is involved in the hydrolysis of retinal.[59,60,62]

Ligand Flexibility Reconciles Active-State Crystal Structures. Our simulation data also help reconcile the contradictory crystal structures of active rhodopsin, in which retinal was found in opposite orientations. Although it is possible that this difference is simply an artifact of crystallization, it could also represent the presence of multiple retinal conformations in the active protein. We suggest that the present finding, that retinal becomes more dynamic as the protein moves from the dark to the Meta I state, supports the latter hypothesis. The ligand's Schiff base-linked lysine was more flexible in the complex-counterion simulation, adopting distinct χ_1 (Cα–Cβ) and Cε–Nζ torsions. Moreover, all Lys296$^{7.43}$ torsions were more dynamic in the complex-counterion simulation than in the dark state. Retinal's increased flexibility after isomerization (Figure 5a) coincides with the intuitive idea that, because Meta I serves as the last intermediate before the protein reaches its active conformation, the system is quite dynamic. Instead of being constrained to the first 400 ns, these torsions fluctuate throughout the complex-counterion simulation, suggesting that the enhanced dynamics are not occurring only during ligand elongation. The orientation of these torsions propagates to retinal and most likely plays an important role in determining the ligand's conformation. Enhanced flexibility suggests retinal has multiple

dx.doi.org/10.1021/bi4013947 | *Biochemistry* 2014, 53, 376–385

conformations in the active state of rhodopsin, permitting the different ligand orientations seen in the recent Meta II structures.[21,22] This observation also helps explain the multiple retinal occupancies reported[21] near the Schiff base linkage.

Besides the changes in Lys296$^{7.43}$, retinal's β-ionone ring made a more subtle transition in the complex-counterion simulation, a reorientation of the C6−C7 torsion (Figure 5a). Initially, this torsion was in the *gauche*− state, which was the primary conformation in the dark-state simulation. In the complex-counterion simulation, it quickly changed to *gauche*+, making several transitions in the first 350 ns and then remaining primarily in the *trans* state. This conformation oriented the C5-methyl toward the extracellular side of rhodopsin for much of the simulation, including the last 500 ns, which were used to calculate the theoretical spectra (see the Supporting Information). Perhaps most striking were the results of principal component analysis, which revealed that the retinal elongation (Figure 5b) and the associated upward translation (Figure 3b) of the β-ionone ring were the most concerted motions in the complex-counterion simulation. This elongation (Figure 5b) occurred primarily 200−450 ns into the trajectory, the same region of the simulation during which the C6−C7 torsion was most dynamic, indicating that this flexibility may be related to ligand elongation.

CONCLUSIONS

We have described the dynamics of retinal in the binding pocket in both the dark and Meta I states using molecular dynamics simulations that were validated by solid-state ^{2}H NMR spectroscopy. Retinal was shown to take on markedly different conformations in the binding pocket after isomerization. In our simulation, the ligand translated toward the extracellular side of the protein, allowing the highly conserved Trp265$^{6.48}$ to undergo a χ_1 torsional rotation. This motion was also accompanied by a surprising influx of bulk water into the hydrophobic core of the protein. Furthermore, we saw differences in ligand torsional states that go well beyond the typical C11=C12 isomerization; the lysine side chain and the β-ionone ring were more dynamic in the complex-counterion simulation. This enhanced torsional flexibility might explain the long-axis flip and structural degeneracy recently reported in the Meta II crystal structures.[21,22] Whether Meta II exists as a single structure or is defined by an ensemble of states will be an important question for future research.

ASSOCIATED CONTENT

Supporting Information

Figures showing a comparison between the experiments, the full experimental data set with the corresponding simulation data, and the χ_2 torsion of the dark-state simulation. This material is available free of charge via the Internet at http://pubs.acs.org.

Web-Enhanced Features

Two videos showing binding pocket motion and internal hydration in the complex-counterion simulation.

AUTHOR INFORMATION

Corresponding Authors

*E-mail: alan_grossfield@urmc.rochester.edu. Phone: (585) 276-4193.

*E-mail: mfbrown@u.arizona.edu. Phone: (520) 621-2163.

Present Addresses

[@]B.M.: C. Eugene Bennett Department of Chemistry, West Virginia University, Morgantown, WV 26506.

[#]K.M.-M.: Instituto de Química, Universidad Nacional Autónoma de México, México City 04510, Mexico.

[∇]M.C.P.: Department of Chemistry and Biochemistry, University of Arizona, Tucson, AZ 85721.

Funding

This work was supported by the National Institutes of Health Grants GM068411 to N.L., EY019614 to B.M., GM095496 to A.G., and EY012049 and EY018891 to M.F.B.

Notes

The authors declare no competing financial interest.

ACKNOWLEDGMENTS

We thank A. Struts and J. Leioatts for helpful discussions about the manuscript and the IBM T. J. Watson Research Center for computing resources.

ABBREVIATIONS

GPCR, G-protein-coupled receptor; Meta I, metarhodopsin I; Meta II, metarhodopsin II; ssNMR, solid-state nuclear magnetic resonance spectroscopy; H*x*, helix *x*; MD, molecular dynamics; PCA, principal component analysis; SDPE, 1-stearoyl-2-docosahexaenoyl-*sn*-glycero-3-phosphoethanolamine; SDPC, 1-stearoyl-2-docosahexaenoyl-*sn*-glycero-3-phosphocholine.

REFERENCES

(1) Fredriksson, R., Lagerström, M. C., Lundin, L.-G., and Schiöth, H. B. (2003) The G-protein-coupled receptors in the human genome form five main families. Phylogenetic analysis, paralogon groups, and fingerprints. *Mol. Pharmacol. 63*, 1256−1272.

(2) Lefkowitz, R. J. (2004) Historical review: A brief history and personal retrospective of seven-transmembrane receptors. *Trends Pharmacol. Sci. 25*, 413−422.

(3) Rosenbaum, D. M., Rasmussen, S. G. F., and Kobilka, B. K. (2009) The structure and function of G-protein-coupled receptors. *Nature 459*, 356−363.

(4) Nygaard, R., Frimurer, T. M., Holst, B., Rosenkilde, M. M., and Schwartz, T. W. (2009) Ligand binding and micro-switches in 7TM receptor structures. *Trends Pharmacol. Sci. 30*, 249−259.

(5) Hubbell, W. L., Altenbach, C., Hubbell, C. M., and Khorana, H. G. (2003) Rhodopsin structure, dynamics, and activation: A perspective from crystallography, site-directed spin labeling, sulfhydryl reactivity, and disulfide cross-linking. *Adv. Protein Chem. 63*, 243−290.

(6) Mombaerts, P. (1999) Seven-transmembrane proteins as odorant and chemosensory receptors. *Science 286*, 707−711.

(7) Firestein, S. (2000) The good taste of genomics. *Nature 404*, 552−553.

(8) Howard, A. D., McAllister, G., Feighner, S. D., Liu, Q., Nargund, R. P., Van der Ploeg, L. H. T., and Patchett, A. A. (2001) Orphan G-protein-coupled receptors and natural ligand discovery. *Trends Pharmacol. Sci. 22*, 132−140.

(9) Overington, J. P., Al-Lazikani, B., and Hopkins, A. L. (2006) How many drug targets are there? *Nat. Rev. Drug Discovery 5*, 993−996.

(10) Bahar, I., Lezon, T. R., Bakan, A., and Shrivastava, I. H. (2010) Normal mode analysis of biomolecular structures: Functional mechanisms of membrane proteins. *Chem. Rev. 110*, 1463−1497.

(11) Granier, S., and Kobilka, B. (2012) A new era of GPCR structural and chemical biology. *Nat. Chem. Biol. 8*, 670−673.

(12) Okada, T., Ernst, O. P., Palczewski, K., and Hofmann, K. P. (2001) Activation of rhodopsin: New insights from structural and biochemical studies. *Trends Biochem. Sci. 26*, 318−324.

(13) Ballesteros, J., and Weinstein, H. (1995) Integrated methods for the construction of three-dimensional models and computational probing of structure-function relations in G protein-coupled receptors. *Methods Neurosci. 25*, 366−428.
(14) Burns, M. E., and Baylor, D. A. (2001) Activation, deactivation, and adaptation in vertebrate photoreceptor cells. *Annu. Rev. Neurosci. 24*, 779−805.
(15) Cooper, A. (1979) Energy uptake in the first step of visual excitation. *Nature 282*, 531−533.
(16) Lewis, J. W., Kliger, D. S., and Krzystof, P. (2000) Absorption spectroscopy in studies of visual pigments: Spectral and kinetic characterization of intermediates. *Meth. Enzymol. 315*, 164−178.
(17) Palczewski, K., Kumasaka, T., Hori, T., Behnke, C. A., Motoshima, H., Fox, B. A., Le Trong, I., Teller, D. C., Okada, T., Stenkamp, R. E., Yamamoto, M., and Miyano, M. (2000) Crystal structure of rhodopsin: A G protein-coupled receptor. *Science 289*, 739−745.
(18) Okada, T., Sugihara, M., Bondar, A.-N., Elstner, M., Entel, P., and Buss, V. (2004) The retinal conformation and its environment in rhodopsin in light of a new 2.2 Å crystal structure. *J. Mol. Biol. 342*, 571−583.
(19) Nakamichi, H., and Okada, T. (2006) Crystallographic analysis of primary visual photochemistry. *Angew. Chem. 45*, 4270−4273.
(20) Nakamichi, H., and Okada, T. (2006) Local peptide movement in the photoreaction intermediate of rhodopsin. *Proc. Natl. Acad. Sci. U.S.A. 103*, 12729−12734.
(21) Standfuss, J., Edwards, P. C., D'Antona, A., Fransen, M., Xie, G., Oprian, D. D., and Schertler, G. F. X. (2011) The structural basis of agonist-induced activation in constitutively active rhodopsin. *Nature 471*, 656−660.
(22) Choe, H.-W., Kim, Y. J., Park, J. H., Morizumi, T., Pai, E. F., Krauß, N., Hofmann, K. P., Scheerer, P., and Ernst, O. P. (2011) Crystal structure of metarhodopsin II. *Nature 471*, 651−655.
(23) Deupi, X., Edwards, P., Singhal, A., Nickle, B., Oprian, D., Schertler, G., and Standfuss, J. (2012) Stabilized G protein binding site in the structure of constitutively active metarhodopsin-II. *Proc. Natl. Acad. Sci. U.S.A. 109*, 119−124.
(24) Scheerer, P., Park, J. H., Hildebrand, P. W., Kim, Y. J., Krauß, N., Choe, H.-W., Hofmann, K. P., and Ernst, O. P. (2008) Crystal structure of opsin in its G-protein-interacting conformation. *Nature 455*, 497−502.
(25) Park, J. H., Scheerer, P., Hofmann, K. P., Choe, H.-W., and Ernst, O. P. (2008) Crystal structure of the ligand-free G-protein-coupled receptor opsin. *Nature 454*, 183−187.
(26) Altenbach, C., Kusnetzow, A. K., Ernst, O. P., Hofmann, K. P., and Hubbell, W. L. (2008) High-resolution distance mapping in rhodopsin reveals the pattern of helix movement due to activation. *Proc. Natl. Acad. Sci. U.S.A. 105*, 7439−7444.
(27) Patel, A. B., Crocker, E., Eilers, M., Hirshfeld, A., Sheves, M., and Smith, S. O. (2004) Coupling of retinal isomerization to the activation of rhodopsin. *Proc. Natl. Acad. Sci. U.S.A. 101*, 10048−10053.
(28) Ruprecht, J. J., Mielke, T., Vogel, R., Villa, C., and Schertler, G. F. X. (2004) Electron crystallography reveals the structure of metarhodopsin I. *EMBO J. 23*, 3609−3620.
(29) Crocker, E., Eilers, M., Ahuja, S., Hornak, V., Hirshfeld, A., Sheves, M., and Smith, S. O. (2006) Location of Trp265 in metarhodopsin II: Implications for the activation mechanism of the visual receptor rhodopsin. *J. Mol. Biol. 357*, 163−172.
(30) Ahuja, S., Crocker, E., Eilers, M., Hornak, V., Hirshfeld, A., Ziliox, M., Syrett, N., Reeves, P. J., Khorana, H. G., Sheves, M., and Smith, S. O. (2009) Location of the retinal chromophore in the activated state of rhodopsin. *J. Biol. Chem. 284*, 10190−10201.
(31) Hornak, V., Ahuja, S., Eilers, M., Goncalves, J. A., Sheves, M., Reeves, P. J., and Smith, S. O. (2010) Light activation of rhodopsin: Insights from molecular dynamics simulations guided by solid-state NMR distance restraints. *J. Mol. Biol. 396*, 510−527.
(32) Struts, A. V., Salgado, G. F. J., and Brown, M. F. (2011) Solid-state ^{2}H NMR relaxation illuminates functional dynamics of retinal cofactor in membrane activation of rhodopsin. *Proc. Natl. Acad. Sci. U.S.A. 108*, 8263−8268.
(33) Struts, A. V., Salgado, G. F. J., Martínez-Mayorga, K., and Brown, M. F. (2011) Retinal dynamics underlie its switch from inverse agonist to agonist during rhodopsin activation. *Nat. Struct. Mol. Biol. 18*, 392−394.
(34) Mertz, B., Lu, M., Brown, M. F., and Feller, S. E. (2011) Steric and electronic influences on the torsional energy landscape of retinal. *Biophys. J. 101*, L17−L19.
(35) Eilers, M., Goncalves, J. A., Ahuja, S., Kirkup, C., Hirshfeld, A., Simmerling, C., Reeves, P. J., Sheves, M., and Smith, S. O. (2012) Structural transitions of transmembrane helix 6 in the formation of metarhodopsin I. *J. Phys. Chem. B 116*, 10477−10489.
(36) Martínez-Mayorga, K., Pitman, M. C., Grossfield, A., Feller, S. E., and Brown, M. F. (2006) Retinal counterion switch mechanism in vision evaluated by molecular simulations. *J. Am. Chem. Soc. 128*, 16502−16503.
(37) Nevzorov, A. A., Moltke, S., Heyn, M. P., and Brown, M. F. (1999) Solid-state NMR line shapes of uniaxially oriented immobile systems. *J. Am. Chem. Soc. 121*, 7636−7643.
(38) Vogel, R., Siebert, F., Yan, E. C. Y., Sakmar, T. P., Hirshfeld, A., and Sheves, M. (2006) Modulating rhodopsin receptor activation by altering the pK_a of the retinal Schiff base. *J. Am. Chem. Soc. 128*, 10503−10512.
(39) Lüdeke, S., Beck, M., Yan, E. C. Y., Sakmar, T. P., Siebert, F., and Vogel, R. (2005) The role of Glu181 in the photoactivation of rhodopsin. *J. Mol. Biol. 353*, 345−356.
(40) Struts, A. V., Salgado, G. F. J., Tanaka, K., Krane, S., Nakanishi, K., and Brown, M. F. (2007) Structural analysis and dynamics of retinal chromophore in dark and meta I states of rhodopsin from ^{2}H NMR of aligned membranes. *J. Mol. Biol. 372*, 50−66.
(41) Grossfield, A., Pitman, M. C., Feller, S. E., Soubias, O., and Gawrisch, K. (2008) Internal hydration increases during activation of the G-protein-coupled receptor rhodopsin. *J. Mol. Biol. 381*, 478−486.
(42) Lau, P.-W., Grossfield, A., Feller, S. E., Pitman, M. C., and Brown, M. F. (2007) Dynamic structure of retinylidene ligand of rhodopsin probed by molecular simulations. *J. Mol. Biol. 372*, 906−917.
(43) Grossfield, A., Feller, S. E., and Pitman, M. C. (2006) A role for direct interactions in the modulation of rhodopsin by ω-3 polyunsaturated lipids. *Proc. Natl. Acad. Sci. U.S.A. 103*, 4888−4893.
(44) Fitch, B. G., Germain, R. S., Mendell, M., Pitera, J., Pitman, M., Rayshubskiy, A., Sham, Y., Suits, F., Swope, W., Ward, T. J. C., Zhestkov, Y., and Zhou, R. (2003) Blue Matter, an application framework for molecular simulation on Blue Gene. *J. Parallel Distrib. Comput. 63*, 759−773.
(45) MacKerell, A. D., Jr., Bashford, D., Bellott, M., Dunbrack, R. L., Jr., Evanseck, J. D., Field, M. J., Fischer, S., Gao, J., Guo, H., Ha, S., Joseph-McCarthy, D., Kuchnir, L., Kuczera, K., Lau, F. T. K., Mattos, C., Michnick, S., Ngo, T., Nguyen, D. T., Prodhom, B., Reiher, W. E., III, Roux, B., Schlenkrich, M., Smith, J. C., Stote, R., Straub, J., Watanabe, M., Wiórkiewicz-Kuczera, J., Yin, D., and Karplus, M. (1998) All-atom empirical potential for molecular modeling and dynamics studies of proteins. *J. Phys. Chem. B 102*, 3586−3616.
(46) Feller, S. E., and MacKerell, A. D., Jr. (2000) An improved empirical potential energy function for molecular simulations of phospholipids. *J. Phys. Chem. B 104*, 7510−7515.
(47) Nina, M., Smith, J. C., and Roux, B. (1993) Ab Initio quantum-chemical analysis of Schiff base-water interactions in bacteriorhodopsin. *J. Mol. Struct. 286*, 231−245.
(48) Andersen, H. C. (1983) Rattle: A "velocity" version of the shake algorithm for molecular dynamics calculations. *J. Comput. Phys. 52*, 24−34.
(49) Essmann, U., Perera, L., Berkowitz, M. L., Darden, T., Lee, H., and Pedersen, L. G. (1995) A smooth particle mesh Ewald method. *J. Chem. Phys. 103*, 8577−8593.
(50) Romo, T. D., and Grossfield, A. (2009) LOOS: An extensible platform for the structural analysis of simulations. *Conf. Proc. IEEE Eng. Med. Biol. Soc. 2009*, 2332−2335.

(51) Grossfield, A., Feller, S. E., and Pitman, M. C. (2007) Convergence of molecular dynamics simulations of membrane proteins. *Proteins: Struct., Funct., Bioinf. 67*, 31−40.
(52) Brooks, B. R., Janežič, D., and Karplus, M. (1995) Harmonic analysis of large systems. I. Methodology. *J. Comput. Chem. 16*, 1522−1542.
(53) Zhu, S., Brown, M. F., and Feller, S. E. (2013) Retinal conformation governs pK_a of protonated Schiff base in rhodopsin activation. *J. Am. Chem. Soc. 135*, 9391−9398.
(54) Hayashi, S., Tajkhorshid, E., and Schulten, K. (2009) Photochemical reaction dynamics of the primary event of vision studied by means of a hybrid molecular simulation. *Biophys. J. 96*, 403−416.
(55) Valsson, O., Campomanes, P., Tavernelli, I., Rothlisberger, U., and Filippi, C. (2013) Rhodopsin absorption from first principles: Bypassing common pitfalls. *J. Chem. Theory Comput. 9*, 2441−2454.
(56) Shi, L., Liapakis, G., Xu, R., Guarnieri, F., Ballesteros, J. A., and Javitch, J. A. (2002) β_2 Adrenergic receptor activation. Modulation of the proline kink in transmembrane 6 by a rotamer toggle switch. *J. Biol. Chem. 277*, 40989−40996.
(57) Schwartz, T. W., Frimurer, T. M., Holst, B., Rosenkilde, M. M., and Elling, C. E. (2006) Molecular mechanism of 7TM receptor activation—a global toggle switch model. *Annu. Rev. Pharmacol. Toxicol. 46*, 481−519.
(58) Huber, T., Botelho, A. V., Beyer, K., and Brown, M. F. (2004) Membrane model for the G-protein-coupled receptor rhodopsin: Hydrophobic interface and dynamical structure. *Biophys. J. 86*, 2078−2100.
(59) Angel, T. E., Gupta, S., Jastrzebska, B., Palczewski, K., and Chance, M. R. (2009) Structural waters define a functional channel mediating activation of the GPCR, rhodopsin. *Proc. Natl. Acad. Sci. U.S.A. 106*, 14367−14372.
(60) Angel, T. E., Chance, M. R., and Palczewski, K. (2009) Conserved waters mediate structural and functional activation of family A (rhodopsin-like) G protein-coupled receptors. *Proc. Natl. Acad. Sci. U.S.A. 106*, 8555−8560.
(61) Nygaard, R., Valentin-Hansen, L., Mokrosinski, J., Frimurer, T. M., and Schwartz, T. W. (2010) Conserved water-mediated hydrogen bond network between TM-I, -II, -VI, and -VII in 7TM receptor activation. *J. Biol. Chem. 285*, 19625−19636.
(62) Jastrzebska, B., Palczewski, K., and Golczak, M. (2011) Role of bulk water in hydrolysis of the rhodopsin chromophore. *J. Biol. Chem. 286*, 18930−18937.